Supplement of Eur. J. Mineral., 35, 1149–1157, 2023
https://doi.org/10.5194/ejm-35-1149-2023-supplement

European Journal of Mineralogy
Open Access

Supplement of

In situ study of the reaction phase A plus high-P clinoenstatite to forsterite plus water at reduced water activity

Christian Lathe et al.

Correspondence to: Christian Lathe (christian.lathe@gfz-potsdam.de)

Supplementary material

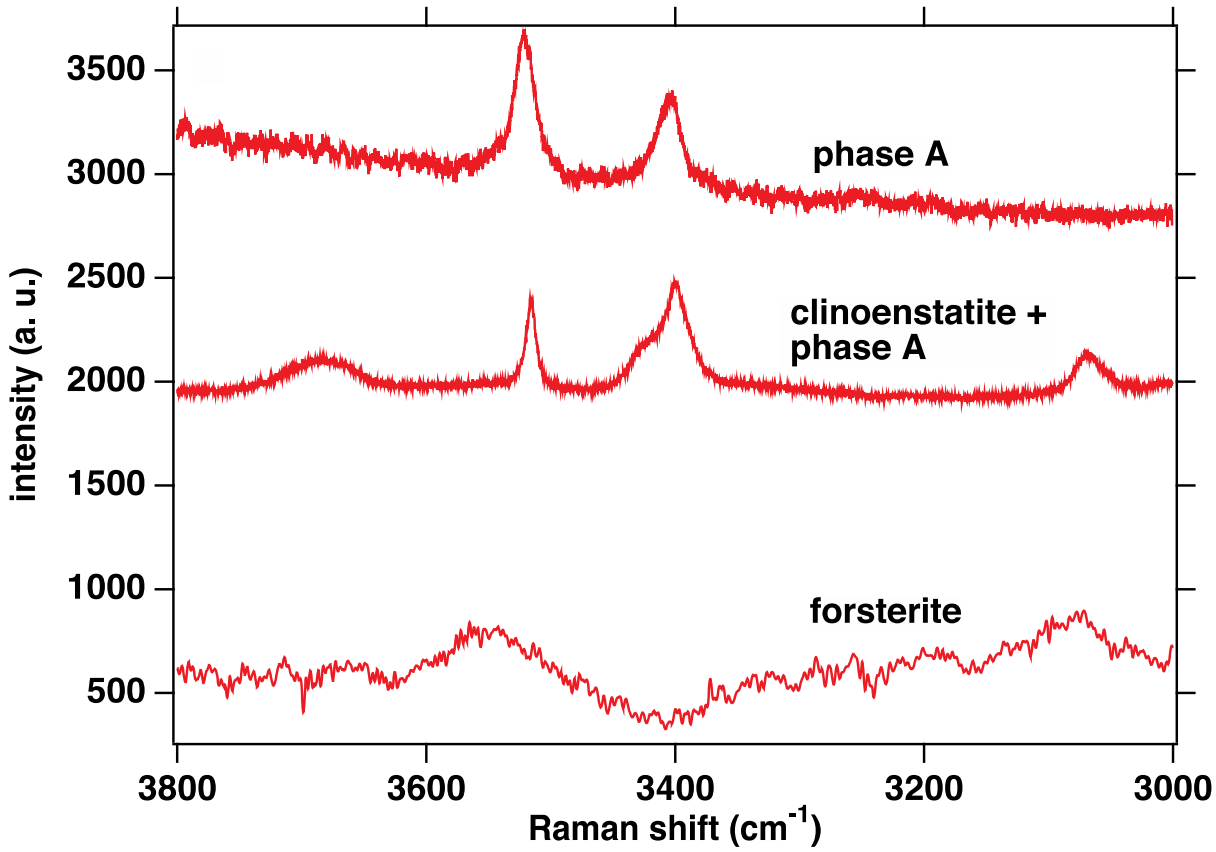

Figure S1. Raman spectra of run products (MA 622 at 10 GPA, 750 °C hold for 4 h) in the OH stretching region: phase A showing the initial OH content and clinoenstatite and forsterite showing OH incorporated during the HP/HT run. Raman spectroscopy is not that sensitive to OH in NAM's as IR but the fact that we see here counts of several 100's for the respective OH peaks means that OH is incorporated as several 100's of ppm H_2O in cen and fo. To quantify this was not the aim of this study.

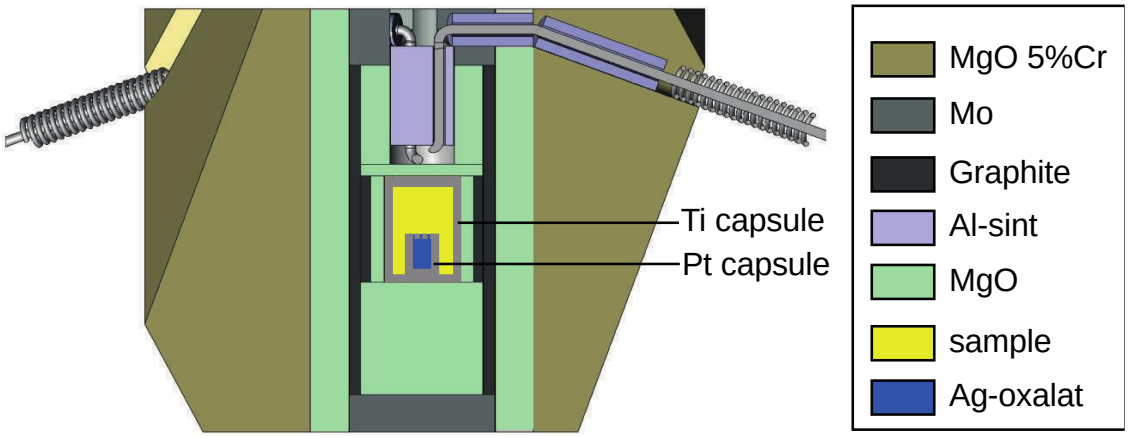

Figure S2. Cartoon of the high-pressure assembly used in the large volume press (LVP) at the synchrotron storage ring of PETRA III in Hamburg (beamline P61B; large volume press with extreme conditions - LVP-ECs). Ti capsule is 2 mm long.

Table S1. Characterisation of the starting materials

Starting materials	*a* (Å)	*b* (Å)	*c* (Å)	*β* °	*V* (Å^3)	Space group
Clinoenstatite[1]	9.607(4)	8.817(3)	5.172(4)	108.35(5)	415.7(5)	$P2_1/c$.
Forsterite[2]	4.7549(1)	10.1958(2)	5.9810(1)	90.00	289.959(9)	*Pbnm*
Phase A[3]	7.8648(3)	7.8648(3)	9.5783(3)	90.00	513.08(3)	$P6_3$.

[1] Clinoenstatite was synthesized at 1 atm heating a $MgSiO_3$-glas at 1500 °C for 3 hours, followed by rapid quenching using the method described by Anderson and Browen (1914). The synthetic clinoenstatite was already described in Wunder and Schreyer (1997): Antigorite: High-pressure stability in the system MgO-SiO_2-H_2O. Lithos, 41, 213-227, 1997.
[2] Synthetic forsterite was provided by the Leibniz-Institut für Kristallzüchtung (IKZ). The sample contained 100 % forsterite.
[3] Phase A was synthesized at 8 GPa, 700 °C, 48 hours using a gel with the Mg/Si-ratio of 7/2 plus water in excess. The sample contained >0.99 wt % phase A and traces of periclase as determined by X-ray diffraction plus Rietveld refinement. Average of 16 electron microprobe analyses: $Mg_{6.89(4)}Si_{2.03(2)}O_{14}H_{6.1}$.

Table S2. Result of the in situ experiment 599 at DESY, including their starting material, experimental conditions, and reaction progress by intensity 1-(I_{at}/I_o) of reflections (110) of ph A and (021) of fo.

Run	Starting material	*P* (GPa)	*T* (°C)	Time (min)	Result (growth of)	ph A 1-(I_{at}/I_o) (110)	fo 1-(I_{at}/I_o) (021)
In situ experiments at DESY							
599	fo, LP-Cen, ph A, H_2O	10.0	700	5	ph A, HP-Cen	0.00	0.00
	fo, LP-Cen, ph A, H_2O	10.0	700	15	ph A, HP-Cen	0.03	-0.09

fo, LP-Cen, ph A, H_2O	10.0	700	35	ph A, HP-Cen	0.07	-0.15
fo, LP-Cen, ph A, H_2O	10.0	700	53	ph A, HP-Cen	0.09	-0.22
fo, LP-Cen, ph A, H_2O	9.7	725	0	fo	0.00	0.00
fo, LP-Cen, ph A, H_2O	9.7	725	30	fo	-0.02	0.01
fo, LP-Cen, ph A, H_2O	9.7	725	60	fo	-0.05	0.03
fo, LP-Cen, ph A, H_2O	9.7	725	90	fo	-0.07	0.05
fo, LP-Cen, ph A, H_2O	9.7	725	122	fo	-0.09	0.06

Abbreviations: fo - forsterite; ph A – phase A; LP-Cen – low-*P* clinoenstatite; HP-Cen – high-*P* clinoenstatite.

Thermodynamic calculations

To constrain the experimentally obtained *P*-*T*-coordinates of the reaction R1 (phase A plus enstatite to olivine plus water) with a CO_2-H_2O fluid, phase diagrams were calculated with Perple_X using a gridded minimization strategy and linear programming for optimization (Connolly, 2005). The calculations were performed in the MgO-SiO_2-CO_2-H_2O-system using the volatile-free bulk composition of the starting material saturated with a CO_2+H_2O fluid (Figure 1). The thermocalc ds6 database, the Holland and Powell (1991) CORK equation of state and the CO_2-H_2O fluid model (Connolly and Trommsdorff, 1991) for the fluid were used. The endmembers brucite, clinohumite, clinoenstatite, chondrodite, coesite, high-pressure enstatite, H_2O liquid, MgO liquid, magnesite and stishovite were excluded from the calculations because they were not overserved in the experiment and/or because the endmembers from the anhydrous mantle (Holland et al., 2013) are not consistent with a fluid. Calculations were performed between 7 and 12 GPa and between 550 and 800 °C for X_{CO_2} = 0.5 and X_{H2O} = 1.

Since those calculations consider a simplified COH-fluid containing only pure species such as CO_2 and H_2O, we also used the deep earth water model (Sverjensky, 2019) which did not provide reasonable results, most likely due to the extrapolation of model-calibration data to the here relevant high pressures.

For calibration, the deep earth water model incorporated various data sources. These include, for instance, aqueous speciation data for carbonate and bicarbonate species (Facq et al., 2014, 2016) and silica monomer and dimer species (Mysen, 2010). In addition, solubility data for individual minerals such as quartz (Manning, 1994) and mineral pairs such as forsterite and enstatite (Newton and Manning, 2002b) were used. It is worth noting that the solubility measurements used in this calibration did not include solubility data for chemical systems more complex than one or two pure minerals and did not exceed 2 GPa, expect for the studies on carbonate and bicarbonate species. Those limitations restrict the applicability of chemical mass transfer (Sverjensky and Huang, 2015; Galvez et al., 2016). Huang and Sverjensky (2019) extended the scope to higher pressure (4-5 GPa) and temperatures (700-1000 °C) including experimental solubility data from complex multicomponent systems, in particular the Na_2O-K_2O-MgO-CaO-Al_2O_3-SiO_2-FeO-H_2O-CO_2-H_2 system, in synthetic eclogites and peridotites. Despite those considerable achievements, the validity of extrapolations to higher pressures, relevant to this study, lacks verification. Indeed, the experimental data for dielectric constant of water is limited to 1200 °C and 6 GPa and due to the lack of basic experimental spectroscopic data on speciation in high-density aqueous liquids, the exact nature of ligands and complexes under high pressure is still very uncertain (Sverjensky 2019).

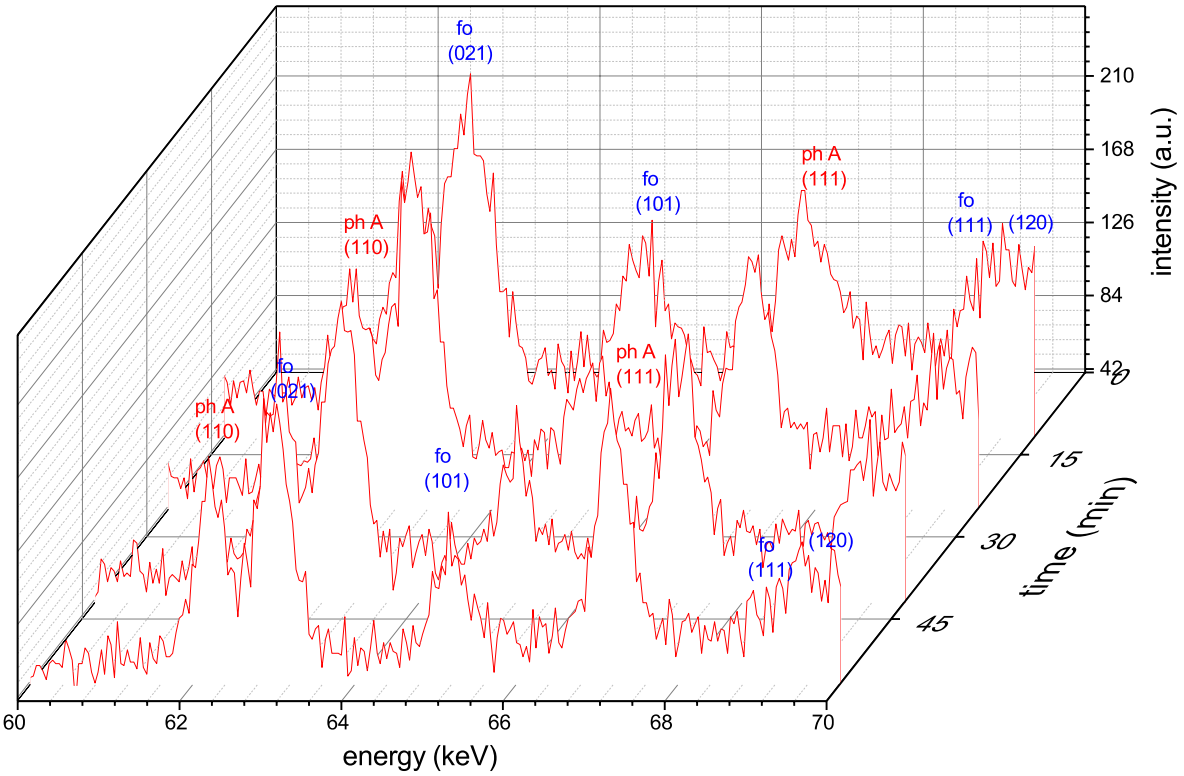

Figure S3. Representative EDX spectra of run 599 (synchrotron) as a function of time taken at 10.0 GPa and 700 °C showing growth of phase A (see also Tab S2).

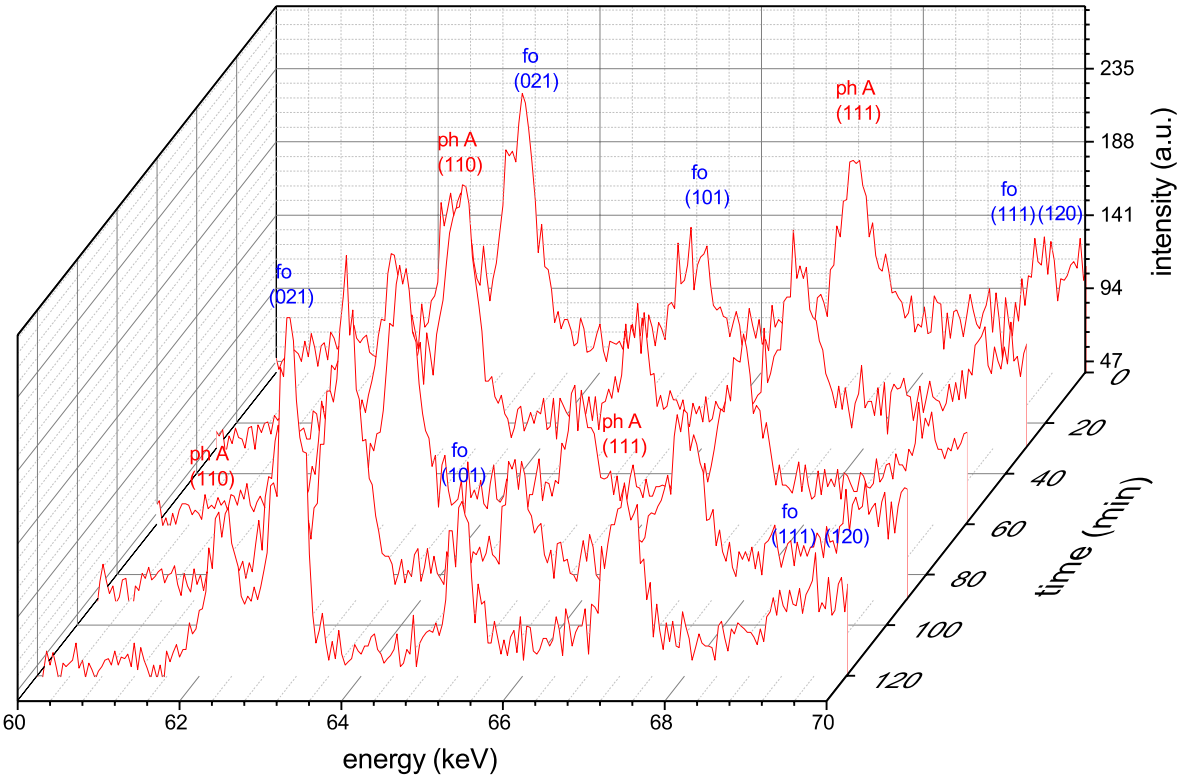

Figure S4. Representative EDX spectra of run 599 (synchrotron) as a function of time taken at 9.7 GPa and 725 °C showing growth of forsterite (see also Tab S2).

References

Connolly, J.A.D.: Computation of phase equilibria by linear programming: A tool for geodynamic modeling and its application to subduction zone decarbonation, Earth Planet. Sci. Lett., 236 (1-2), 524–541, DOI: 10.1016/j.epsl.2005.04.033, 2005.

Connolly, J.A.D. and Trommsdorff, V.: Petrogenetic grids for metacarbonate rocks: pressure-temperature phase-diagram projection for mixed-volatile systems, Contrib. Mineral. Petrol., 108 (1), 93–105, DOI: 10.1007/BF00307329, 1991.

Facq, S., Daniel, I., Montagnac, G., Cardon, H., and Sverjensky, D.A.: In situ Raman study and thermodynamic model of aqueous carbonate speciation in equilibrium with aragonite under subduction zone conditions. Geochim. Cosmochim. Ac., 132, 375–390, 2014.

Facq, S., Daniel, I., Montagnac, G., Cardon, H., and Sverjensky, D.A.: Carbon speciation in saline solutions in equilibrium with aragonite at high pressure. Chem. Geol., 431, 44–53, DOI: 10.1016/j.chemgeo.2016.03.021, 2016.

Hacker, B., Abers, G. and Peacock, S.: Subduction factory 1. Theoretical mineralogy, densities and seismic wave speeds, and H_2O contents, J. Geophys. Res., 108, 2029, https://doi.org/10.1029/2001JB001127, 2003.

Huang, F., and Sverjensky, D.A.: Extended Deep Earth Water Model for predicting major element mantle metasomatism. Geochim. Cosmochim.Ac., 254, 192–230, DOI: 10.1016/j.gca.2019.03.027, 2019.

Holland, T. and Powell, R.: A compensated-Redlich-Kwong (CORK) equation for volumes and fugacities of CO2 and H2O in the range 1 bar to 50 kbar and 100–1600C, Contrib. Mineral. Petrol., 109 (2), 265–273, 1991.

Holland, T.J., Hudson, N.F., Powell, R., and Harte, B.: New Thermodynamic Models and Calculated Phase Equilibria in NCFMAS for Basic and Ultrabasic Compositions through the Transition Zone into the Uppermost Lower Mantle, J. Petrol., 54 (9), 1901–1920, DOI: 10.1093/petrology/egt035, 2013.

Galvez, M.E., Connolly, J.A.D., and Manning, C.E.: Implications for metal and volatile cycles from the pH of subduction zone fluids. Nature, 539 (7629), 420–424, DOI: 10.1038/nature20103, 2016.

Manning, C.E.: The solubility of quartz in H2O in the lower crust and upper mantle. Geochim. Cosmochim. Ac., 58 (22), 4831–4839, DOI: 10.1016/0016-7037(94)90214-3, 1994.

Mysen, B.O.: Speciation and mixing behavior of silica-saturated aqueous fluid at high temperature and pressure. Am. Min, 95 (11-12), 1807–1816, DOI: 10.2138/am.2010.3539, 2010.

Newton, R.C., and Manning, C.E.: Solubility of enstatite + forsterite in H2O at deep crust/upper mantle conditions: 4 to 15 kbar and 700 to 900°c. Geochim. Cosmochim. Ac., 66 (23), 4165–4176, DOI: 10.1016/S0016-7037(02)00998-5, 2002.

Sverjensky, D.A.: Thermodynamic modelling of fluids from surficial to mantle conditions. J. Geol. Soc., 176 (2), 348–374, DOI: 10.1144/jgs2018-105, 2019.

Sverjensky, D.A., and Huang, F.: Diamond formation due to a pH drop during fluid–rock interactions. Nat. Commun., 6 (1), 8702, DOI: 10.1038/ncomms9702, 2015.